Radiology

Molecular Body Imaging: MR Imaging, CT, and US. Part I. Principles[1]

Moritz F. Kircher, MD
Jürgen K. Willmann, MD

Molecular imaging, generally defined as noninvasive imaging of cellular and subcellular events, has gained tremendous depth and breadth as a research and clinical discipline in recent years. The coalescence of major advances in engineering, molecular biology, chemistry, immunology, and genetics has fueled multi- and interdisciplinary innovations with the goal of driving clinical noninvasive imaging strategies that will ultimately allow disease identification, risk stratification, and monitoring of therapy effects with unparalleled sensitivity and specificity. Techniques that allow imaging of molecular and cellular events facilitate and go hand in hand with the development of molecular therapies, offering promise for successfully combining imaging with therapy. While traditionally nuclear medicine imaging techniques, in particular positron emission tomography (PET), PET combined with computed tomography (CT), and single photon emission computed tomography, have been the molecular imaging methods most familiar to clinicians, great advances have recently been made in developing imaging techniques that utilize magnetic resonance (MR), optical, CT, and ultrasonographic (US) imaging. In the first part of this review series, we present an overview of the principles of MR imaging-, CT-, and US-based molecular imaging strategies.

[1] From the Department of Radiology, Memorial Sloan-Kettering Cancer Center, New York, NY (M.F.K.); and Department of Radiology and Molecular Imaging Program at Stanford, Stanford University School of Medicine, 300 Pasteur Dr, Room H1307, Stanford, CA 94305-5621 (J.K.W.). Received December 13, 2010; revision requested January 14, 2011; revision received August 10; accepted September 13; final version accepted November 10. **Address correspondence to** J.K.W. (e-mail: *willmann@stanford.edu*).

In the past 3 decades, the use of noninvasive imaging for disease diagnosis has seen a tremendous growth spurt and has become an indispensable component of clinical practice. Today, imaging systems that provide anatomic and limited physiologic information are in widespread clinical use. Such systems include computed tomography (CT), magnetic resonance (MR) imaging, and ultrasonography (US) (1).

Although CT offers high patient throughput and high-resolution imaging, molecular information is difficult to extract from CT images, as the images are based solely on differences in x-ray attenuation. Similarly, clinically used US currently offers cost-effective organ evaluation without radiation exposure, but its signal is generated by sound wave reflection and perturbation, which does not usually provide information on the underlying molecular composition of tissue. While the physical basis of MR imaging is fundamentally molecular in nature, the majority of current MR protocols in the clinic use MR imaging to provide gross anatomic or functional information. Relatively few pulse sequences and protocols have been developed that actually enable assessment of specific cellular or subcellular events without the use of molecular contrast agents. These include, for example, MR spectroscopy and diffusion-weighted imaging, which provide information on the molecular composition of the tissue and water diffusion, respectively (2,3).

By contrast, for example, positron emission tomography (PET), in conjunction with suitable PET radiotracers, represents a true molecular imaging technique that has been in routine clinical use for many years. However, not only is PET expensive and of limited availability, but current PET scanners yield low spatial resolution compared with that of CT, MR imaging, and US; therefore, PET data must be combined with data from a second modality such as CT or MR imaging to provide anatomic detail.

While PET technology has improved incrementally over the years, entirely new molecular imaging techniques and molecular probes have been developed, many of which are currently being tested in preclinical or clinical trials, and some are already in clinical evaluation at selected academic centers (1,4–9). These include, for example, nontargeted and targeted (10), as well as activatable MR (11–14) and optical probes (15); endoscopic (16,17) and intraoperative optical devices (18–20); ultrasonic molecular imaging (21); photoacoustic imaging (22); and Raman spectroscopy (9,23).

The purpose of this review is to highlight recent molecular imaging approaches that use technologies applied in routine clinical radiologic practice, including MR imaging, CT, and US, and have potential for clinical translation in the future. In the first part of the review we outline the underlying principles of these approaches, and in the second part we will describe their applications.

Essentials

- While PET represents the mainstay of molecular imaging in the current clinical practice, several other imaging approaches hold promise for translation in the near future.
- There are a large variety of different mechanisms that can create molecular MR contrast agents, which have progressively evolved in their sensitivity; activatable and other "smart" MR probe concepts promise to increase specificity.
- While the literature on molecular CT principles is still sparse, several nanoparticle approaches show promise for further development.
- Molecular imaging principles in US often rely on the design of molecularly-targeted microbubbles, but nanoparticle-based contrast agents are also evolving.

Molecular MR Imaging

Because of its inherently low sensitivity in depicting contrast agents, MR imaging is a less than ideal imaging modality for target-specific imaging. While its sensitivity (10^{-3}–10^{-5} M for most contrast agents) (24) for detection of contrast agent is superior to that of CT (not well characterized, approximate estimation, 10^{-1}–10^{-2} M) (24,25), it is orders of magnitude lower than that of PET (10^{-11}–10^{-12} M) (24) or US detection of microbubbles (10^{-12} M) (26). However, given the marked advances that have been made in the design and chemistry of MR imaging contrast agents, molecular imaging using MR has become a reality (27). Molecular MR imaging contrast agents are usually based on nanoparticulate probes that contain a high payload of contrast-generating metals (eg, iron oxide nanoparticles or nanoscaffolds loaded with gadolinium chelates [Gd^{3+}]) and are aimed at a molecular target by, for example, a binding ligand attached to the contrast agent. Target-specific contrast agents are a particular challenge for MR imaging given its low sensitivity, but several concepts that exploit amplification strategies may overcome this problem. In the following section, different principles by which molecular MR contrast can be generated are discussed.

Principles of MR Contrast Agents

T2 and T1 Contrast Agents

Agents that are used to create contrast enhancement on T2-weighted images usually are superparamagnetic iron oxide nanoparticles, which are composed of a core of iron oxide measuring 3–5 nm, coated with dextran, starch, polymer, or citrate (28). The development

Published online
10.1148/radiol.12102394 **Content code:** MI

Radiology 2012; 263:633–643

Abbreviations:
CLIO = cross-linked iron oxide
PARACEST = paramagnetic chemical exchange saturation transfer
USPIO = ultrasmall superparamagnetic iron oxide

Funding:
This research was supported by the National Institutes of Health (grant R21 CA139279).

Potential conflicts of interest are listed at the end of this article.

Figure 1

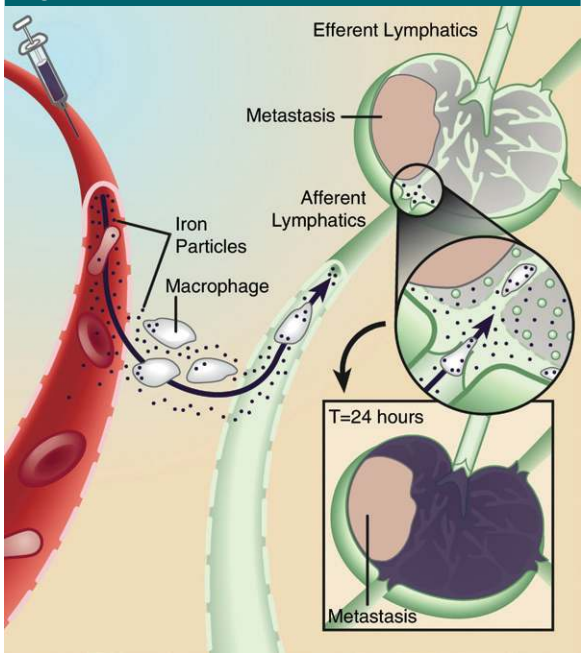

Figure 1: Mechanism of action for lymphotropic superparamagnetic nanoparticles, one of the first clinically used cellular MR contrast agents. Systemically injected particles gain access to the interstitium and are drained through lymphatic vessels. In a normal lymph node, iron oxide nanoparticles are taken up by phagocytic cells, which cause the lymph node to become dark on T2-weighted images due to susceptibility artifacts from iron. If a lymph node is partially or fully replaced by metastatic cells, fewer nanoparticles are retained in the lymph node, which therefore remains bright on T2-weighted images. (Adapted and reprinted, with permission, from reference 36)

Figure 2

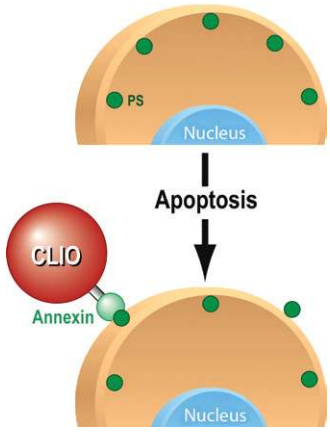

Figure 2: Mechanism of action for targeted MR molecular contrast agent for apoptosis imaging. As one of the early changes that occur when cells undergo apoptosis, phosphatidylserines (*PS,* green circles) become externalized on the cell membrane. Annexin V, conjugated to an iron oxide nanoparticle (CLIO), recognizes and binds to the externalized phosphatidylserines, leading to accumulation of the contrast agent; there is consecutive detectable signal intensity change on MR images.

of these nanoparticles dates back to the 1980s and has since undergone continued refinement. While initial preparations such as Feridex (Advanced Magnetics, Cambridge, Mass) used thin dextran coatings, subsequent versions featured a more extensive polymer coating and remained monodisperse in vivo (monodisperse iron oxide nanoparticles, or MION) (29). The latter also have a smaller hydrodynamic diameter, which led to the more general term ultrasmall superparamagnetic iron oxide (USPIO) for this and other similar iron oxide nanoparticles with a size of less than 50 nm. Further advances introduced particle stabilization via cross-linking of its dextran coating, leading to the experimental nanoparticle cross-linked iron oxide (CLIO) (30). Featuring amination of the coating, CLIO also allows straightforward conjugation of additional moieties such as near-infrared fluorochromes to yield multimodality nanoparticles (31–33) and/or multiple ligands to yield multivalent, targeted nanoparticles (34,35).

USPIO and CLIO are long-circulating particles (blood half-life of approximately 24 hours) that are removed from the circulation by the reticuloendothelial system (36) (Fig 1). Given their long half-life and small size of approximately 30 nm, they are able to penetrate tissues of interest such as myocardium, atherosclerotic plaques, or tumors. Their high relaxivity (R2 of USPIO at 0.5 T: 50 $[mmol/L]^{-1} \cdot sec^{-1}$, R2 of CLIO: up to 150 $[mmol/L]^{-1} \cdot sec^{-1}$ [37]) allows detection of sparsely expressed targets with sufficient sensitivity for in vivo detection (28). These nanoparticles can be targeted toward a specific receptor or molecule of interest by conjugating ligands such as antibodies, peptides, or small molecules to their surface (Fig 2).

T1 contrast agents usually consist of chelates of paramagnetic metal ions, most commonly Gd^{3+}, which exhibits a high magnetic moment due to its seven unpaired electrons. The detection threshold of gadolinium chelates has been in the micromolar range and thus is substantially lower than that of iodinated contrast agents commonly used in CT, which is estimated to be in the range of hundreds of millimolar to molar concentrations. However, many molecular targets of interest are expressed in the low nanomolar range, and therefore the detection sensitivity of routinely used gadolinium chelates is inadequate for molecular MR imaging in most cases. To address these limitations, several new gadolinium constructs have been developed. Examples include gadolinium-con-

taining dendrimers (38) (particles containing a core and a branched, tree-like surface structure), micelles (39) (phospholipid monolayer with hydrophilic surface and hydrophobic core), gadolinium-containing liposomes (40) (phospholipid bilayers with a core of fluid encapsulated by a hydrophobic membrane), and gadolinium-containing perfluorocarbon emulsions (41) or high-density lipoprotein-like nanoparticles (42). These newer particles possess both longer intravascular half-lives and higher longitudinal relaxivities (r1) (r1 values of most clinically approved gadolinium chelates are approximately 4 $[mmol/L]^{-1} \cdot sec^{-1}$, whereas r1 values of new gadolinium particles range between 10 and 20 $[mmol/L]^{-1} \cdot sec^{-1}$)(28,41). This, in combination with high numbers of gadolinium chelates per particle, can enable detection in the picomolar range (particle concentration) and, therefore, enable visualization with MR imaging of sparse binding sites (41).

Contrast Agents Based on Fluorine 19

While in most MR imaging applications water protons (hydrogen 1 [^{1}H]) are used to create contrast enhancement, other nuclei can also be used to provide contrast enhancement on MR images. Because of its low natural abundance and high gyromagnetic ratio, fluorine 19 [^{19}F] is particularly well suited for this purpose. Nanoparticles that contain high numbers of ^{19}F atoms have been developed and can be used as contrast agents (43). The key advantage of using ^{19}F instead of ^{1}H is that the endogenous presence of ^{19}F in the body is negligible, which results in the absence of undesired tissue background signal. Therefore, the recorded signal on the MR image unequivocally originates from the ^{19}F in the contrast agent. By superimposing the ^{19}F signal on regular ^{1}H MR images, the anatomic location of the ^{19}F signal can be precisely determined (43,44).

Chemical Exchange Saturation Transfer Agents

A newer class of paramagnetic contrast agents is based on the magnetization transfer method. Contrast agents used for this purpose are called chemical exchange saturation transfer, or CEST, agents. MR imaging based on the magnetic transfer method is reviewed in more detail elsewhere (45). Briefly, these new agents produce MR imaging contrast enhancement in a fundamentally different way, in that contrast enhancement is not based on proton relaxation, but instead on selectively reducing the magnetization of the water signal, with only minimal effect on its longitudinal relaxation rate. CEST agents rely on the presence of at least two pools of protons with different nuclear MR chemical shifts. One pool (pool A) contains the contrast agent with its exchangeable protons; the other pool (pool B) contains bulk water. If a frequency-selective radiofrequency pulse is applied that saturates the proton spins in pool A, an exchange of protons from pool A to pool B during this saturation period leads to a decrease in the intensity of the spins in pool B and thus to a decrease in MR signal (45,46). When these agents contain paramagnetic lanthanides such as dysprosium ion (Dy^{3+}), terbium ion (Tb^{3+}), thulium ion (Tm^{3+}), or ytterbium ion (Yb^{3}+), they are called PARACEST agents (45,47,48). In contradistinction to conventional gadolinium- or iron-based contrast agents, which affect T1 and T2 relaxation, imaging signal with use of PARACEST agents can be enhanced more specifically: Only if the excitation radiofrequency is set at the value that corresponds to the absorption frequency of their mobile protons do they display an effect on image signal (46). In addition, this technique enables distinction of two separate PARACEST contrast agents in the same MR experiment, and, therefore, the potential to target two or more molecular markers simultaneously (multiplexing) (48). More recently, PARACEST agents based on liposomes containing the paramagnetic lanthanide complex Tm-DOTMA^{-} have been introduced. These so-called LIPOCEST agents contain a higher number of exchangeable protons per particle, which results in a lower detection threshold in the picomolar range (particle concentration) (50–52).

Activatable MR Contrast Agents

A subset of MR molecular imaging contrast agents, also known as activatable MR imaging probes, are designed to elicit a detectable change in signal in response to the local environment, and thus are able to "sense" specific molecular states. A first generation of such agents was based on the principle of a chemical reaction that completely changes the nature of the final contrast agent (53). In contrast, a second generation of agents undergoes a change in relaxivity, while the basic topology of the contrast agent remains unchanged. These agents often have an "off" state associated with low relaxivity in the absence of an external stimulus and an "on" state associated with high relaxivity in the presence of the stimulus. These types of contrast agents are also referred to as "smart" contrast agents since they only induce an imaging signal when a particular disease state is present (53).

Although there are many different principles by which relaxivity of MR contrast agents can be changed probably one of the most attractive driving forces in contrast agent activation is based on the ability of certain enzymes to form or cleave bonds, given the relevance of enzymatic activity as indicators of certain disease states. Several applications of enzyme-sensing probes have been described, with β-galactosidase–sensitive paramagnetic substrates having been described early on. In the landmark study by Louie et al (12), the β-galactosidase–sensitive probe is inactive in its native form, where the access of water to Gd^{3+} is blocked by a residue. The enzyme β-galactosidase cleaves off the blocking residue, which allows Gd^{3+} to directly interact with water protons. This subsequently causes an irreversible increase in the T1 signal. While such approaches are based on the ability of certain enzymes to break specific chemical bonds, the limitation is that they are only applicable to hydrolases, that is, enzymes that exhibit hydrolytic activity. In a different activation mechanism, oppositely acting enzymes (eg, polymerases) catalyze chemical bond formation (53). The substrates consist of chelated gadolinium

covalently bound to phenols, which then serve as electron donors during enzymatic hydrogen peroxide reduction by peroxidase. The converted monomers undergo rapid condensation into paramagnetic oligomers, which leads to a threefold increase in relaxivity (54). In a modification of this principle, serotonin functions as a reducing substrate for myeloperoxidase, an enzyme that is related to inflammation (11,13,14,55) (Fig 3).

Superparamagnetic iron oxide particles have also been used to design activatable MR probes. These probes make use of a unique magnetic phenomenon, termed magnetic relaxation switching: When individual magnetic nanoparticles undergo self-assembly into larger nanoassembly clusters, the result is more efficient dephasing of spins in the surrounding water protons and, thus, a measurable increase in spin-spin (T2) relaxation times (56). This mechanism has been exploited as a tool for detecting biomolecules in homogeneous assays and has demonstrated detection limits as low as 500 amol (56–59).

More recently, activatable PARACEST agents have been developed. Depending on the design of these probes, enzymatic cleavage of a substrate initiates either the loss of the PARACEST signal (60) ("switch off") or the appearance of the PARACEST signal (61) ("switch on"). While both activatable superparamagnetic and PARACEST agents show great promise in vitro, their potential for robust in vivo applications still needs to be studied further.

Multimodality Probes

The purpose of multimodality imaging probes is to combine the advantages of complimentary modalities. Usually the goal is to achieve both high spatial resolution and high sensitivity (eg, by combining MR imaging with nuclear imaging) or to allow both preoperative staging and intraoperative molecular imaging (eg, by combining MR imaging with optical imaging) (23,32). For example, when an iron oxide core is combined with activatable optical components such as fluorochromes, a single probe can now be depicted with high spatial resolution in deep tissues (via MR imaging) and at the same time deliver information on the activity of specific enzymes (by means of optical imaging of enzymatically activatable fluorochromes) (31,33,62) (Fig 4). Another recently reported concept of a multimodal probe is the use of MR imaging for preoperative staging and the use of optical imaging methods such as Raman spectroscopic imaging for ultrasensitive tumor resection (23). Since MR imaging is a modality that offers depth-independent high-spatial-resolution detection, it represents a common platform for multimodality probes.

Figure 3

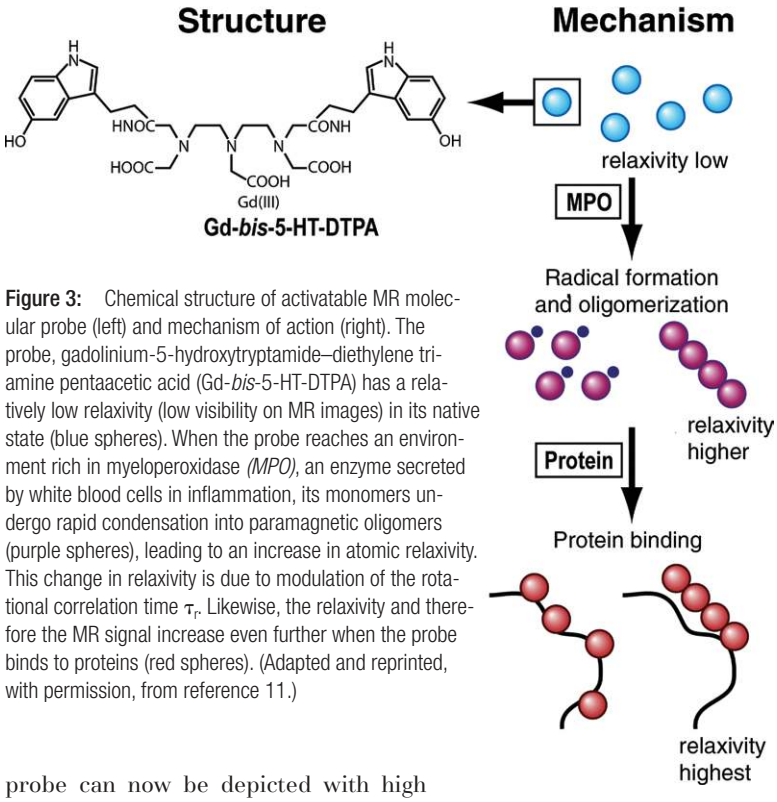

Figure 3: Chemical structure of activatable MR molecular probe (left) and mechanism of action (right). The probe, gadolinium-5-hydroxytryptamide–diethylene triamine pentaacetic acid (Gd-*bis*-5-HT-DTPA) has a relatively low relaxivity (low visibility on MR images) in its native state (blue spheres). When the probe reaches an environment rich in myeloperoxidase *(MPO)*, an enzyme secreted by white blood cells in inflammation, its monomers undergo rapid condensation into paramagnetic oligomers (purple spheres), leading to an increase in atomic relaxivity. This change in relaxivity is due to modulation of the rotational correlation time τ_r. Likewise, the relaxivity and therefore the MR signal increase even further when the probe binds to proteins (red spheres). (Adapted and reprinted, with permission, from reference 11.)

Hyperpolarization

A principle entirely different from the ones described earlier is the basis of a method called hyperpolarization. This technique was devised to address the realization that MR imaging provides unsurpassed soft-tissue contrast enhancement but, in comparison to other imaging modalities, is relatively insensitive because of the intrinsically low sensitivity of the MR phenomenon. The underlying principle of MR imaging is based on the interaction of atomic nuclei with an external magnetic field. Nuclear spins can orient themselves in two possible directions: parallel ("spin-up") or antiparallel ("spin-down") to the external field (B_0) (Fig 5). If the two populations are equal, their magnetic moments cancel, resulting in no MR signal. In thermal equilibrium (Fig 5a), there are a very small number of unequally oriented spins ($\sim$ 1 in 10^5), resulting in low sensitivity (63). The idea of hyperpolarization (Fig 5b) is to create an artificial nonequilibrium of spins, which can enhance the MR sensitivity by a factor of 10000 or more (64). This strong signal enhancement enables imaging of nuclei other than protons of even lower abundance, for example, carbon 13 (^{13}C) and nitrogen 15, and allows their molecular distribution to be followed in vivo with short imaging times (62). This enables visualization of metabolic processes noninvasively in vivo (65). A hyperpolarized

Figure 4

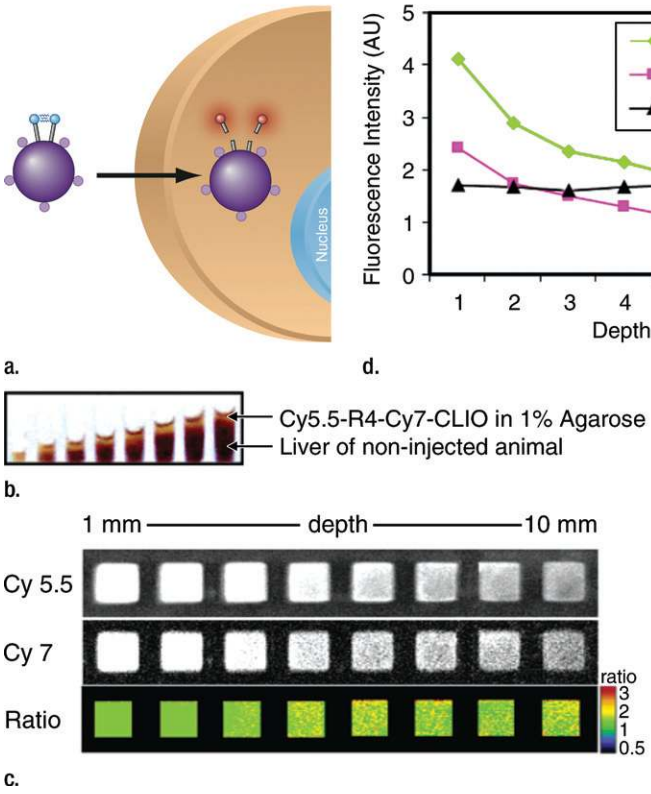

Figure 4: **(a)** Mechanism of action for dual-modality, activatable, magneto-optical molecular imaging MR contrast agent, which consists of a core of a dextran-coated iron oxide nanoparticle, onto which fluorochrome A (small purple spheres) is conjugated. Also attached to its surface are peptides carrying a second fluorochrome B (blue spheres) that can be cleaved by a specific enzyme. When the contrast agent enters an environment where the specific enzyme is present (eg, cathepsin B, which is overexpressed in breast cancer), the fluorochrome-carrying peptides are cleaved and thus fluorochrome B detaches. The increased distance of the fluorochromes causes dequenching, resulting in increased fluorescence signal. The intensity of fluorochrome A remains the same. **(b–d)** Illustration of fluorescence ratio method. Fluorescence is normally depth dependent and difficult to quantify. However, if two fluorochromes are used, where one is nonactivatable and serves as an internal standard, correction for depth is possible. While the signal from both fluorochromes used here (Cy5.5 and Cy7) decreases with increasing depth, the ratio of the two signal intensities remains the same (**c, d**). (Images **b–d** reprinted, with permission, from reference 33.)

state of molecules can be created in vivo by means of dynamic nuclear polarization techniques, such as the so-called Overhauser effect, in combination with a suitable contrast agent (66). Alternatively, hyperpolarization of an imaging agent can be induced by an external device, followed by immediate administration of the hyperpolarized agent into the organism of interest. Examples of the latter technique include hyperpolarization of the noble gases helium 3 (67) and xenon 129 (68) by using optical pumping or hyperpolarization of various organic molecules containing ^{13}C by using either parahydrogen (69) or dynamic nuclear polarization techniques (70).

Molecular CT Imaging

CT is an imaging modality that is widely available, relatively cost-effective, and enables high-resolution whole-body imaging with unparalleled speed. In addition, its resultant image data representing attenuation values of tissues is highly quantifiable, which has resulted in its use as a method to correct for attenuation of other modalities such as PET. Given these attributes, CT may in principle serve as a very suitable platform for molecular imaging. However, its main limitation is its low sensitivity and limited soft-tissue contrast. Soft-tissue contrast in CT is dependent on the mass attenuation coefficient of the tissue and can be enhanced by injecting a contrast agent. Current CT contrast agents are based on small iodinated molecules. These are effective in absorbing x-rays, but their rapid pharmacokinetics and nonspecific distribution limit their use as targeted agents. As a result, there is renewed interest in the development of engineered nanomaterials as CT contrast agents.

Principles of Molecular CT Contrast Agents

The principle of CT as a method that measures x-ray absorption requires the use of materials containing high-atomic-number (Z) elements to increase image contrast and, thus, the sensitivity of CT imaging for detection of targeted contrast agents. In addition to the clinically used iodine, the element gold has received much attention. Other CT molecular imaging agents contain bismuth sulfide, as well as composite ceramics containing iron oxide and lanthanide materials. Most CT molecular contrast agents are designed to incorporate a maximum number of x-ray–absorbing atoms into a nanoparticle, with designs ranging from emulsions (71–73) (Fig 6), liposomes (74), and lipoproteins (42) to polymeric nanoparticles (75,76). A key feature of many of these nanoparticle designs is their pharmacokinetics, which are often markedly different than those of small iodinated molecules in clinical use. For example, the circulation time can be increased dramatically, as was shown for a bismuth sulfide nanoparticle agent (77), for which the circulation time is longer than 2 hours. Increasing the circulation time has implications for targeting of contrast agents, because longer circulation times increase the chance of interaction and binding of a contrast agent to a target.

Figure 5

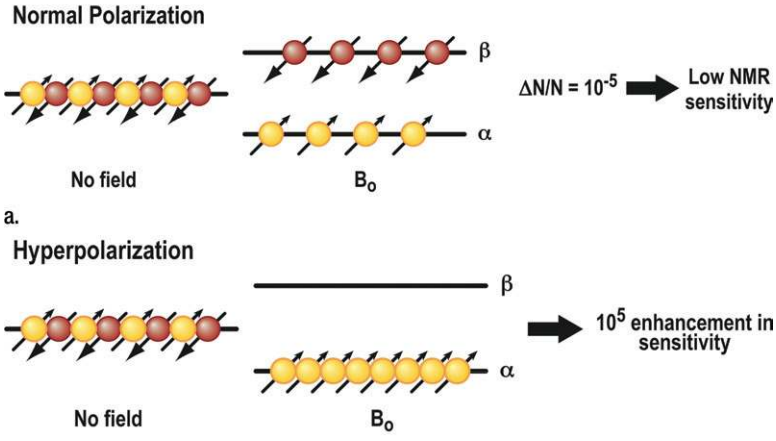

Figure 5: Mechanism of action for MR hyperpolarization. The fundamental principle of MR imaging is based on the interaction of atomic nuclei with an external magnetic field. **(a)** Nuclei can orient themselves in two possible directions: parallel ("spin up," α) or antiparallel ("spin-down," β) to the external field (B_0). If the two populations are equal, their magnetic moments cancel, resulting in no MR signal. In thermal equilibrium, there are a very small number of unequally oriented spins (~ 1 in 10^5). Only this small number of spins can contribute to the MR signal, resulting in a low sensitivity. **(b)** The idea of hyperpolarization is to create an artificial nonequilibrium of spins. This means that the number of unequally oriented spins will be increased by a factor of up to 100 000, which therefore results in a much higher MR signal.

Figure 6

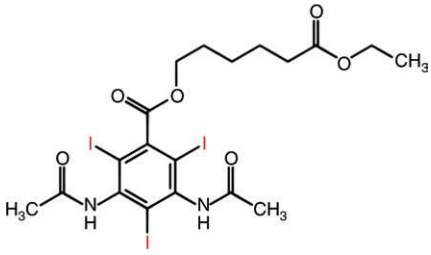

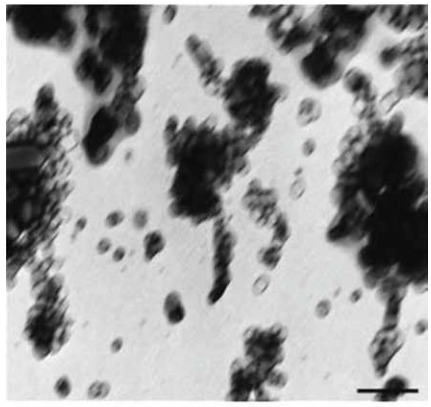

Figure 6: Principle of a nanoparticulate CT contrast agent. **(a)** Schematic representation of the contrast-generating iodinated compound of the nanoparticle CT contrast agent N1177 containing three iodine *(I)* atoms (red). **(b)** Electron microscopy image of N1177. The nanoparticles are suspensions of crystalline iodinated compound, combined with biocompatible surfactants to prevent aggregation and stabilize nanoparticle size. Shown are electron-dense iodinated granules coated by polymers appearing as negative prints after staining with a solution of uranyl acetate. Nanoparticles have various sizes and shapes. Scale bar = 100 nm. (Adapted and reprinted, with permission, from reference 72.)

Molecular US Imaging

In the past decade, targeted contrast-enhanced US imaging (molecular US) has emerged as a new noninvasive molecular imaging strategy. Its main advantage is the ability to extract molecular information in addition to the known advantages of US, including portability, cost-effectiveness, absence of ionizing irradiation, high spatial and temporal resolution (real-time examination), and global availability (78,79). Molecular US allows semiquantitative and quantitative assessment of molecular target expression with very high sensitivity, and the combination of the latest US hardware with advances in contrast agent design is expected to further increase the likelihood of clinical translation in the near future (78,80).

Principles of Molecular US Contrast Agents

There are currently two main classes of US contrast agents: *(a)* microbubble-based agents and *(b)* non–microbubble-based agents (78,81) (Fig 7). Microbubbles represent gas-liquid emulsions, which consist of a gaseous core surrounded by a shell with a size of approximately 1–4 μm. The gaseous core, when insonified by the sound beam, causes a high echogenic response resulting in high contrast-to-background–tissue ratio (78). Furthermore, US detection of microbubbles exploits the nonlinear behavior of microbubbles, which compress and expand in an acoustic field close to their resonance frequency, resulting in nonlinear scattering of sound to frequencies two times or more above (harmonics) or below (subharmonics) the input frequency (5). Frequency filtering of the nonlinear (caused by the resonance of the microbubbles) and linear signals allows sensitive detection of the imaging signal caused by microbubbles, compared with the suppressed background tissue signal. In clinical US imaging systems, different frequencies have been implemented (eg, the pulse-inversion technique) to separate imaging signal from microbubbles and the surrounding tissue signal (5). Microbubbles with different characteristics have been synthesized by combining different shell compositions with different gaseous cores. The microbubble shell can be manufactured of polymers, albumin, galactose (82), or lipids, while either air or high-molecular-weight gases (perfluorocarbon or sulfur hexafluoride) are used as gas cores (83). Grafted arms of polyethylene glycol can be incorporated into the shell surface to add stearic protection and prevent microbubble aggregation (84). A specific characteristic of micro-

Figure 7

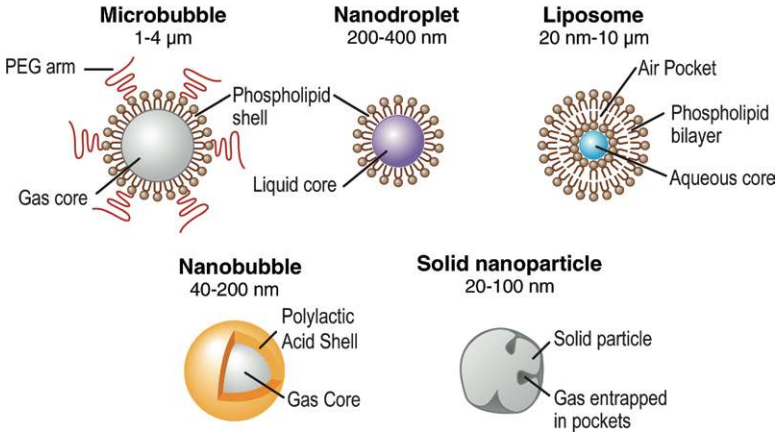

Figure 7: Overview of different types of US contrast agents. Microbubbles are gas-liquid emulsions with a polyethylene glycol *(PEG)* polymer on their surface to prevent aggregation. Perfluorocarbon emulsion nanodroplets are liquid-liquid emulsions that can be vaporized into echogenic gas bubbles after administration of acoustic energy. Liposomes are phospholipid bilayers that can enclose air pockets for US imaging. Nanobubbles are gas-liquid emulsions that can fuse into echogenic microbubbles at the target site. Solid nanoparticles are solid amorphous substances with gas entrapped in their pores or fissures, which increases their echogenicity. (Adapted and reprinted, with permission, from reference 85.)

bubbles is their relatively large size, which prevents them from leaking into the extravascular space. This property can be exploited for imaging by targeting the microbubbles (Fig 8) to disease processes reflected on the vascular endothelial cells lining the luminal surface of capillaries and vessels, such as inflammation and angiogenesis (both tumor angiogenesis and therapeutic angiogenesis) (78,80). Multitargeted microbubbles can be synthetized and have been shown to exhibit increased binding efficiency (Fig 9).

Non–microbubble-based contrast agents (Fig 7), because of their smaller size, have the ability to enter the extravascular space, enabling imaging of targets outside the vascular compartment. These particles consist of either liquid or solid colloids and range in size between 10 and 1000 nm. Different types of non-microbubble particles, with varying sizes and compositions, have been synthesized and have recently been discussed elsewhere in more detail (78). Echogenic liposomes consist of an aqueous core surrounded by a lipid bilayer. Air pockets within the lipid bilayer generate acoustic reflexivity. Perfluorocarbon (PFC) emulsion nanodroplets are 200–400-nm liquid-liquid emulsions consisting of a perfluorocarbon core and a phospholipid monolayer capsule. While individual particles cannot be detected with US, accumulation of a large number of PFC nanodroplets can become acoustically detectable. The liquid core of PFC nanodroplets can also be vaporized into gas by using acoustic energy, leading to substantially increased echogenicity of the particles (78). Nanobubbles are even smaller (40–200-nm) gas-liquid emulsions with a biodegradable polymer shell that have been used mostly for nontargeted passive drug delivery. Solid nanoparticles are amorphous particles that usually consist of silica or iron oxide and contain small gas pockets in their fissures and pores that can generate detectable backscatter for US imaging (Fig 7).

Quantification of Molecular US Imaging Signal By Using US Contrast Microbubbles

Because the imaging signal in contrast-enhanced US is proportional to the concentration or number of the injected microbubbles (86), it is possible to follow either an absolute or a relative approach for quantifying microbubbles in molecular US imaging (78). Absolute quantification of the number of microbubbles at the target site represents the more challenging approach. It requires the calibration of the US system for detected US signal power corresponding to a given number of microbubbles for a particular combination of system settings (eg, dynamic range, gain, mechanical index, etc). The tissue attenuation and the geometry of the imaging beam must be accounted for and are not always known in an in vivo scenario. Furthermore, the effect of nonspecific binding of targeted microbubbles to endothelial cells has to be characterized, and the interaction between the microbubble and vascular endothelial cells must be better understood so that the amount of cellular expression can be inferred from a known number of microbubbles per cell surface marker. These types of corrections have been proposed for imaging of blood perfusion with microbubbles (87) and could potentially be applied to molecular US imaging. However, accounting for all of the parameters mentioned above is complex, and therefore absolute measures of molecular expression with US have not yet been widely adopted.

The relative quantification approach, in contrast, is more straightforward and allows levels of microbubble attachment to be correlated with levels of expression of molecular markers in a semiquantitative fashion. Its underlying principle is the comparison of molecular signal, M (root-mean-square value of the signal within the region), between regions in an image, resulting in a relative value of molecular expression. The signal from two regions, 1 and 2, can be expre.ssed as: $M = M_1/M_2$. The equation relates the amount of molecular signal expressed in region 1 relative to the amount in region 2 as a percentage increase or decrease over time, rather than calculating an absolute quantity of cellular expression. If the regions of interest are in a similar depth range on the image, then differences relating to attenuation

Figure 8

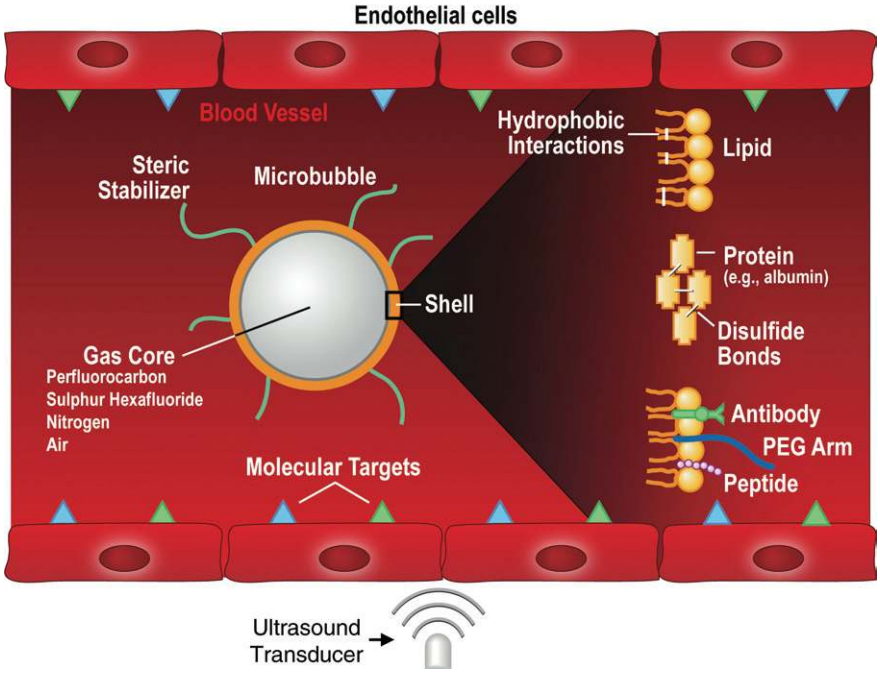

Figure 8: Mechanism of action for targeted US microbubbles. Targeted microbubbles consist of a gas core that can contain different types of gas (eg, perfluorocarbons or nitrogen) surrounded by a shell of, for example, phospholipids or proteins. The microbubble shell can be functionalized by attaching binding ligands such as antibodies or small peptides, which allows the microbubbles to accumulate at sites that overexpress molecular targets (blue and green triangles). Because the size of microbubbles is of several micrometers, they stay exclusively within the vascular compartment, which makes them most useful for imaging and quantification of molecular targets that are luminally overexpressed on vascular endothelial cells, such as markers of angiogenesis or inflammation. When exposed to an ultrasound field, the microbubbles oscillate and send out nonlinear acoustic signals that can be detected with currently clinically used US systems. Since the imaging signal from microbubbles is substantially higher than the signal from surrounding tissue, microbubble accumulation can be imaged with high signal-to-background ratio. *PEG* = polyethylene glycol. (Adapted and reprinted, with permission, from reference 85.)

Figure 9

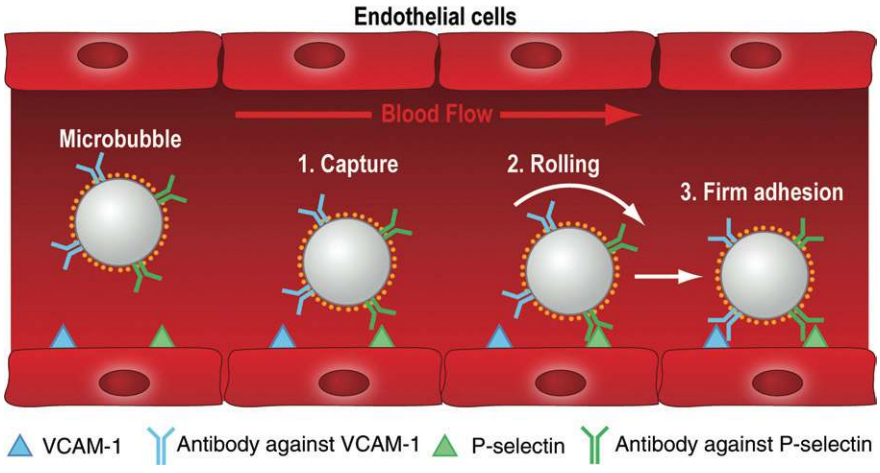

Figure 9: Mechanism of action for dual-targeted microbubbles. Dual-targeted microbubbles can be designed to mimic the behavior of leukocytes in vivo. The diagram shows a dual-targeted microbubble targeted against both P-selectin and vascular cell adhesion molecule-1 *(VCAM-1)*, simulating vascular attachment of a leukocyte at sites of inflammation by first interacting with P-selectin and then firmly attaching via VCAM1. (Adapted and reprinted, with permission, from reference 78.)

and ultrasound beam geometry can be considered negligible, as both *M*1 and *M*2 are affected equally and are effectively cancelled in the equation (78). This relative quantification approach is currently used by the majority of investigators in molecular microbubble imaging research.

Following this introduction into the principles of molecular imaging with MR, CT, and US, the second part of this review series will appear in a future issue of *Radiology* and will focus on in vivo molecular imaging applications.

Acknowledgements: We thank Ralph Weissleder, MD, PhD, Lee Josephson, PhD, John Chen, MD, PhD (all at Massachusetts General Hospital/Harvard Medical School) and Brian Rutt, PhD (Stanford University), for critical review of the manuscript, James Strommer, BA, for help with the figure design and Ada Muellner, MS, for editing the manuscript.

Disclosures of Potential Conflicts of Interest: **M.F.K.** No potential conflicts of interest to disclose. **J.K.W.** No potential conflicts of interest to disclose.

References

1. Weissleder R, Pittet MJ. Imaging in the era of molecular oncology. Nature 2008; 452(7187):580–589.
2. Mazaheri Y, Shukla-Dave A, Muellner A, Hricak H. MRI of the prostate: clinical relevance and emerging applications. J Magn Reson Imaging 2011;33(2):258–274.
3. Vargas HA, Akin O, Franiel T, et al. Diffusion-weighted endorectal MR imaging at 3 T for prostate cancer: tumor detection and assessment of aggressiveness. Radiology 2011; 259(3):775–784.
4. Biswal S, Resnick DL, Hoffman JM, Gambhir SS. Molecular imaging: integration of molecular imaging into the musculoskeletal imaging practice. Radiology 2007;244(3):651–671.

5. Pysz MA, Willmann JK. Targeted contrast-enhanced ultrasound: an emerging technology in abdominal and pelvic imaging. Gastroenterology 2011;140(3):785–790.
6. Kircher MF, Gambhir SS, Grimm J. Noninvasive cell-tracking methods. Nat Rev Clin Oncol 2011;8(11):677–688.
7. Pysz MA, Gambhir SS, Willmann JK. Molecular imaging: current status and emerging strategies. Clin Radiol 2010;65(7):500–516.
8. Willmann JK, van Bruggen N, Dinkelborg LM, Gambhir SS. Molecular imaging in drug development. Nat Rev Drug Discov 2008; 7(7):591–607.
9. Zavaleta CL, Kircher MF, Gambhir SS. Raman's "effect" on molecular imaging. J Nucl Med 2011;52(12):1839–1844.
10. Islam T, Josephson L. Current state and future applications of active targeting in malignancies using superparamagnetic iron oxide nanoparticles. Cancer Biomark 2009;5(2): 99–107.
11. Chen JW, Querol Sans M, Bogdanov A Jr, Weissleder R. Imaging of myeloperoxidase in mice by using novel amplifiable paramagnetic substrates. Radiology 2006;240(2):473–481.
12. Louie AY, Hüber MM, Ahrens ET, et al. In vivo visualization of gene expression using magnetic resonance imaging. Nat Biotechnol 2000;18(3):321–325.
13. Nahrendorf M, Sosnovik D, Chen JW, et al. Activatable magnetic resonance imaging agent reports myeloperoxidase activity in healing infarcts and noninvasively detects the antiinflammatory effects of atorvastatin on ischemia-reperfusion injury. Circulation 2008;117(9):1153–1160.
14. Ronald JA, Chen JW, Chen Y, et al. Enzyme-sensitive magnetic resonance imaging targeting myeloperoxidase identifies active inflammation in experimental rabbit atherosclerotic plaques. Circulation 2009;120(7):592–599.
15. Elias DR, Thorek DL, Chen AK, Czupryna J, Tsourkas A. In vivo imaging of cancer biomarkers using activatable molecular probes. Cancer Biomark 2008;4(6):287–305.
16. Buchner AM, Shahid MW, Heckman MG, et al. Comparison of probe-based confocal laser endomicroscopy with virtual chromoendoscopy for classification of colon polyps. Gastroenterology 2010;138(3):834–842.
17. Wolfsen HC. New technologies for imaging of Barrett's esophagus. Surg Oncol Clin N Am 2009;18(3):487–502.
18. Gibbs-Strauss SL, Rosenberg M, Clough BL, Troyan SL, Frangioni JV. First-in-human clinical trials of imaging devices: an example from optical imaging. Conf Proc IEEE Eng Med Biol Soc 2009;2009:2001–2004.
19. Matsui A, Tanaka E, Choi HS, et al. Real-time intra-operative near-infrared fluorescence identification of the extrahepatic bile ducts using clinically available contrast agents. Surgery 2010;148(1):87–95.
20. Troyan SL, Kianzad V, Gibbs-Strauss SL, et al. The FLARE intraoperative near-infrared fluorescence imaging system: a first-in-human clinical trial in breast cancer sentinel lymph node mapping. Ann Surg Oncol 2009;16(10): 2943–2952.
21. Willmann JK, Lutz AM, Paulmurugan R, et al. Dual-targeted contrast agent for US assessment of tumor angiogenesis in vivo. Radiology 2008;248(3):936–944.
22. De la Zerda A, Zavaleta C, Keren S, et al. Carbon nanotubes as photoacoustic molecular imaging agents in living mice. Nat Nanotechnol 2008;3(9):557–562.
23. Kircher MF, De la Zerda A, Jokerst J, et al. A brain tumor molecular imaging strategy using a novel triple-modality nanoparticle. Nat Med (in press).
24. Massoud TF, Gambhir SS. Molecular imaging in living subjects: seeing fundamental biological processes in a new light. Genes Dev 2003;17(5):545–580.
25. Frangioni JV, Hajjar RJ. In vivo tracking of stem cells for clinical trials in cardiovascular disease. Circulation 2004;110(21): 3378–3383.
26. Klibanov AL, Rasche PT, Hughes MS, et al. Detection of individual microbubbles of ultrasound contrast agents: imaging of free-floating and targeted bubbles. Invest Radiol 2004;39(3):187–195.
27. Aime S, Cabella C, Colombatto S, Geninatti Crich S, Gianolio E, Maggioni F. Insights into the use of paramagnetic Gd(III) complexes in MR-molecular imaging investigations. J Magn Reson Imaging 2002;16(4):394–406.
28. Sosnovik DE, Nahrendorf M, Weissleder R. Molecular magnetic resonance imaging in cardiovascular medicine. Circulation 2007; 115(15):2076–2086.
29. Shen T, Weissleder R, Papisov M, Bogdanov A Jr, Brady TJ. Monocrystalline iron oxide nanocompounds (MION): physicochemical properties. Magn Reson Med 1993;29(5): 599–604.
30. Wunderbaldinger P, Josephson L, Weissleder R. Crosslinked iron oxides (CLIO): a new platform for the development of targeted MR contrast agents. Acad Radiol 2002; 9(Suppl 2):S304–S306.
31. Kircher MF, Josephson L, Weissleder R. Ratio imaging of enzyme activity using dual wavelength optical reporters. Mol Imaging 2002;1(2):89–95.
32. Kircher MF, Mahmood U, King RS, Weissleder R, Josephson L. A multimodal nanoparticle for preoperative magnetic resonance imaging and intraoperative optical brain tumor delineation. Cancer Res 2003;63(23):8122–8125.
33. Kircher MF, Weissleder R, Josephson L. A dual fluorochrome probe for imaging proteases. Bioconjug Chem 2004;15(2):242–248.
34. Kircher MF, Allport JR, Graves EE, et al. In vivo high resolution three-dimensional imaging of antigen-specific cytotoxic T-lymphocyte trafficking to tumors. Cancer Res 2003;63(20):6838–6846.
35. Zhao M, Kircher MF, Josephson L, Weissleder R. Differential conjugation of tat peptide to superparamagnetic nanoparticles and its effect on cellular uptake. Bioconjug Chem 2002;13(4):840–844.
36. Harisinghani MG, Barentsz J, Hahn PF, et al. Noninvasive detection of clinically occult lymph-node metastases in prostate cancer. N Engl J Med 2003;348(25):2491–2499.
37. Högemann-Savellano D, Bos E, Blondet C, et al. The transferrin receptor: a potential molecular imaging marker for human cancer. Neoplasia 2003;5(6):495–506.
38. Swanson SD, Kukowska-Latallo JF, Patri AK, et al. Targeted gadolinium-loaded dendrimer nanoparticles for tumor-specific magnetic resonance contrast enhancement. Int J Nanomedicine 2008;3(2):201–210.
39. Mulder WJ, Strijkers GJ, van Tilborg GA, Griffioen AW, Nicolay K. Lipid-based nanoparticles for contrast-enhanced MRI and molecular imaging. NMR Biomed 2006; 19(1):142–164.
40. Ghaghada KB, Ravoori M, Sabapathy D, Bankson J, Kundra V, Annapragada A. New dual mode gadolinium nanoparticle contrast agent for magnetic resonance imaging. PLoS ONE 2009;4(10):e7628.
41. Morawski AM, Winter PM, Crowder KC, et al. Targeted nanoparticles for quantitative imaging of sparse molecular epitopes with MRI. Magn Reson Med 2004;51(3):480–486.
42. Skajaa T, Cormode DP, Falk E, Mulder WJ, Fisher EA, Fayad ZA. High-density lipoprotein-based contrast agents for multimodal imaging of atherosclerosis. Arterioscler Thromb Vasc Biol 2010;30(2):169–176.
43. Ahrens ET, Flores R, Xu H, Morel PA. In vivo imaging platform for tracking immunotherapeutic cells. Nat Biotechnol 2005;23(8):983–987.
44. Kadayakkara DK, Janjic JM, Pusateri LK, Young WB, Ahrens ET. In vivo observation of intracellular oximetry in perfluorocarbon-labeled glioma cells and chemotherapeutic response in the CNS using fluorine-19 MRI. Magn Reson Med 2010;64(5):1252–1259.
45. Hancu I, Dixon WT, Woods M, Vinogradov E, Sherry AD, Lenkinski RE. CEST and PARACEST MR contrast agents. Acta Radiol 2010;51(8):910–923.
46. Ward KM, Aletras AH, Balaban RS. A new class of contrast agents for MRI based on proton chemical exchange dependent satura-

tion transfer (CEST). J Magn Reson 2000; 143(1):79–87.

47. Woods M, Woessner DE, Sherry AD. Paramagnetic lanthanide complexes as PARACEST agents for medical imaging. Chem Soc Rev 2006;35(6):500–511.
48. Zhang S, Merritt M, Woessner DE, Lenkinski RE, Sherry AD. PARACEST agents: modulating MRI contrast via water proton exchange. Acc Chem Res 2003;36(10):783–790.
49. Aime S, Carrera C, Delli Castelli D, Geninatti Crich S, Terreno E. Tunable imaging of cells labeled with MRI-PARACEST agents. Angew Chem Int Ed Engl 2005;44(12):1813–1815.
50. Aime S, Delli Castelli D, Lawson D, Terreno E. Gd-loaded liposomes as T1, susceptibility, and CEST agents, all in one. J Am Chem Soc 2007;129(9):2430–2431.
51. Aime S, Delli Castelli D, Terreno E. Highly sensitive MRI chemical exchange saturation transfer agents using liposomes. Angew Chem Int Ed Engl 2005;44(34):5513–5515.
52. Delli Castelli D, Dastrù W, Terreno E, et al. In vivo MRI multicontrast kinetic analysis of the uptake and intracellular trafficking of paramagnetically labeled liposomes. J Control Release 2010;144(3):271–279.
53. Querol M, Bogdanov A Jr. Environment-sensitive and enzyme-sensitive MR contrast agents. Handb Exp Pharmacol 2008;(185 Pt 2):37–57.
54. Bogdanov A Jr, Matuszewski L, Bremer C, Petrovsky A, Weissleder R. Oligomerization of paramagnetic substrates result in signal amplification and can be used for MR imaging of molecular targets. Mol Imaging 2002; 1(1):16–23.
55. Rodríguez E, Nilges M, Weissleder R, Chen JW. Activatable magnetic resonance imaging agents for myeloperoxidase sensing: mechanism of activation, stability, and toxicity. J Am Chem Soc 2010;132(1):168–177.
56. Perez JM, Josephson L, O'Loughlin T, Högemann D, Weissleder R. Magnetic relaxation switches capable of sensing molecular interactions. Nat Biotechnol 2002;20(8):816–820.
57. Perez JM, Simeone FJ, Saeki Y, Josephson L, Weissleder R. Viral-induced self-assembly of magnetic nanoparticles allows the detection of viral particles in biological media. J Am Chem Soc 2003;125(34):10192–10193.
58. Grimm J, Perez JM, Josephson L, Weissleder R. Novel nanosensors for rapid analysis of telomerase activity. Cancer Res 2004;64(2): 639–643.
59. Perez JM, Grimm J, Josephson L, Weissleder R. Integrated nanosensors to determine levels and functional activity of human telomerase. Neoplasia 2008;10(10):1066–1072.
60. Yoo B, Pagel MDA. A PARACEST MRI contrast agent to detect enzyme activity. J Am Chem Soc 2006;128(43):14032–14033.
61. Chauvin T, Durand P, Bernier M, et al. Detection of enzymatic activity by PARACEST MRI: a general approach to target a large variety of enzymes. Angew Chem Int Ed Engl 2008;47(23):4370–4372.
62. Josephson L, Kircher MF, Mahmood U, Tang Y, Weissleder R. Near-infrared fluorescent nanoparticles as combined MR/optical imaging probes. Bioconjug Chem 2002;13(3): 554–560.
63. Golman K, Olsson LE, Axelsson O, Månsson S, Karlsson M, Petersson JS. Molecular imaging using hyperpolarized 13C. Br J Radiol 2003;76(Spec No 2):S118–S127.
64. Kurhanewicz J, Vigneron DB, Brindle K, et al. Analysis of cancer metabolism by imaging hyperpolarized nuclei: prospects for translation to clinical research. Neoplasia 2011;13(2):81–97.
65. Viale A, Aime S. Current concepts on hyperpolarized molecules in MRI. Curr Opin Chem Biol 2010;14(1):90–96.
66. Golman K, Petersson JS, Ardenkjaer-Larsen JH, et al. Dynamic in vivo oxymetry using overhauser enhanced MR imaging. J Magn Reson Imaging 2000;12(6):929–938.
67. Middleton H, Black RD, Saam B, et al. MR imaging with hyperpolarized 3He gas. Magn Reson Med 1995;33(2):271–275.
68. Albert MS, Cates GD, Driehuys B, et al. Biological magnetic resonance imaging using laser-polarized 129Xe. Nature 1994;370(6486): 199–201.
69. Golman K, Axelsson O, Jóhannesson H, Månsson S, Olofsson C, Petersson JS. Parahydrogen-induced polarization in imaging: subsecond (13)C angiography. Magn Reson Med 2001;46(1):1–5.
70. Ardenkjaer-Larsen JH, Fridlund B, Gram A, et al. Increase in signal-to-noise ratio of > 10,000 times in liquid-state NMR. Proc Natl Acad Sci USA 2003;100(18):10158–10163.
71. de Vries A, Custers E, Lub J, van den Bosch S, Nicolay K, Grüll H. Block-copolymer-stabilized iodinated emulsions for use as CT contrast agents. Biomaterials 2010;31(25): 6537–6544.
72. Hyafil F, Cornily JC, Feig JE, et al. Noninvasive detection of macrophages using a nanoparticulate contrast agent for computed tomography. Nat Med 2007;13(5):636–641.
73. Kong WH, Lee WJ, Cui ZY, et al. Nanoparticulate carrier containing water-insoluble iodinated oil as a multifunctional contrast agent for computed tomography imaging. Biomaterials 2007;28(36):5555–5561.
74. Elrod DB, Partha R, Danila D, Casscells SW, Conyers JL. An iodinated liposomal computed tomographic contrast agent prepared from a diiodophosphatidylcholine lipid. Nano medicine 2009;5(1):42–45.
75. Aviv H, Bartling S, Kiesling F, Margel S. Radiopaque iodinated copolymeric nanoparticles for x-ray imaging applications. Biomaterials 2009;30(29):5610–5616.
76. Galperin A, Margel D, Baniel J, Dank G, Biton H, Margel S. Radiopaque iodinated polymeric nanoparticles for x-ray imaging applications. Biomaterials 2007;28(30):4461–4468.
77. Rabin O, Manuel Perez J, Grimm J, Wojtkiewicz G, Weissleder R. An x-ray computed tomography imaging agent based on long-circulating bismuth sulphide nanoparticles. Nat Mater 2006;5(2):118–122.
78. Deshpande N, Needles A, Willmann JK. Molecular ultrasound imaging: current status and future directions. Clin Radiol 2010; 65(7):567–581.
79. Hwang M, Lyshchik A, Fleischer AC. Molecular sonography with targeted microbubbles: current investigations and potential applications. Ultrasound Q 2010;26(2):75–82.
80. Kiessling F, Huppert J, Palmowski M. Functional and molecular ultrasound imaging: concepts and contrast agents. Curr Med Chem 2009;16(5):627–642.
81. Deshpande N, Pysz MA, Willmann JK. Molecular ultrasound assessment of tumor angiogenesis. Angiogenesis 2010;13(2):175–188.
82. Cheng KT. Sonicated human serum microspheres. Molecular Imaging and Contrast Agent Database. Bethesda, Md: MICAD, 2004.
83. Klibanov AL. Molecular imaging with targeted ultrasound contrast microbubbles. Ernst Schering Res Found Workshop 2005 (49): 171–191.
84. Walday P, Tolleshaug H, Gjøen T, et al. Biodistributions of air-filled albumin microspheres in rats and pigs. Biochem J 1994; 299(Pt 2):437–443.
85. Deshpande N, Willmann JK. Microparticle- and nanoparticle-based contrast-enhanced ultrasound imaging. In: Chen X, ed. Nanoplatform-based molecular imaging. Hoboken, NJ: Wiley, 2011. doi:10.1002/9780470767047.ch11.
86. de Jong N, Hoff L. Ultrasound scattering properties of Albunex microspheres. Ultrasonics 1993;31(3):175–181.
87. Arditi M, Frinking PJ, Zhou X, Rognin NG. A new formalism for the quantification of tissue perfusion by the destruction replenishment method in contrast ultrasound imaging. IEEE Trans Ultrason Ferroelectr Freq Control 2006;53(6):1118–1129.